Supplementary file

Spatially resolved normal and shear loading beneath stabilised filter-beds on a plain-weave standalone screen

Razqan Razak, Paula A. Gago, Zhixi Chen, Stephen Tyson, Sheikh S. Rahman*

School of Minerals and Energy Resources Engineering, University of New South Wales, Sydney, NSW 2052, Australia

E-mail address: razqanrazak@gmail.com (R. Razak); paulaalejandrayo@gmail.com (P. A. Gago); zhixic@unsw.edu.au (Z. Chen); profstevetyson@protonmail.com (S. Tyson); sheik.rahman@unsw.edu.au (S. S. Rahman).

*Corresponding author (ORCID: 0000-0002-9018-774X (S. S. Rahman))

Razak, R., Gago, P. A., Chen, Z., Tyson, S., Rahman, S. S. Spatially resolved normal and shear loading beneath stabilised filter-beds on a plain-weave standalone screen. Advances in Geo-Energy Research, 2026, 20(2): 114-128.

The link to this file is: https://doi.org/10.46690/ager.2026.05.02

Appendix A: Supplementary materials, geometry, and stabilisation diagnostics

This appendix provides supporting materials that complement the main-paper results. Fig. S1 shows the particle-size distribution used in all cases. The injected sand spans 120 to 630 µm and has a modal diameter near 275 µm. The same distribution was retained for the 180 µm nominal-aperture plain-weave screen. Table S1 lists the imposed pressure drops and the corresponding pressure gradients. Table S2 summarises the computational-domain dimensions and the mean stabilised filter-bed thickness for each case.

Figs. S2 and S3 report the streamwise coordination diagnostics used as supporting checks on the stabilised skeleton subset, defined by $c_{\mathrm{contactno}} \geq 2$. Fig. S2 shows the conditional mean coordination number, $E[c \mid \tilde{x}]$, as a function of the normalised streamwise coordinate $\tilde{x}$, together with the number of skeleton particles per $\tilde{x}$ bin on the secondary axis. Fig. S3 shows the corresponding conditional exceedance fraction, $P(c \geq 10 \mid \tilde{x})$, again together with the bin support on the secondary axis. Global pooling over $\tilde{x}$ and time gives mean coordination numbers of 4.703, 4.607, and 4.602 for Δp_1, Δp_2, and Δp_3, with a common median of 4 and an interquartile range of 3 in all cases. The corresponding far-tail fractions $P(c \geq 10)$ are 0.03335, 0.02794, and 0.02129.

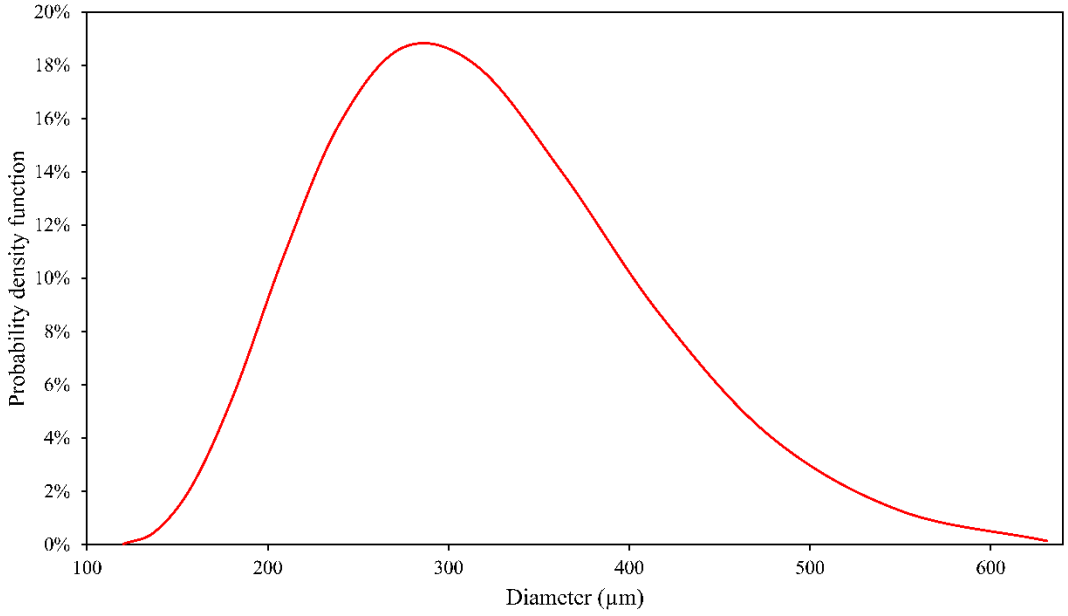

Fig. S1. Particle-size distribution of the injected sand used in all cases.

Table S1. Imposed pressure drops and corresponding pressure gradients.

Case	Δp (Pa)	L_x (m)	$\Delta p / L_x$ (Pa/m)
Δp_1	150	3×10^{-2}	5.0×10^3
Δp_2	450		1.5×10^4
Δp_3	900		3.0×10^4

Table S2. Computational-domain dimensions and mean stabilised filter-bed thickness.

Quantity	Δp_1	Δp_2	Δp_3
Domain length (streamwise), L_x (m)	3×10^{-2}		
Domain width (y), L_y (m)	3.82748×10^{-3}		
Domain depth (z), L_z (m)	3.43964×10^{-3}		
Nominal aperture width (μm)	180		
Mean filter-bed thickness, $\bar{h}$ (m)	9.25×10^{-4}	9.53×10^{-4}	9.42×10^{-4}

The cross-sectional dimensions in the transverse directions are taken from the validated plain-weave configuration, whereas the mean stabilised filter-bed thickness is reported only as a stabilised-state descriptor.

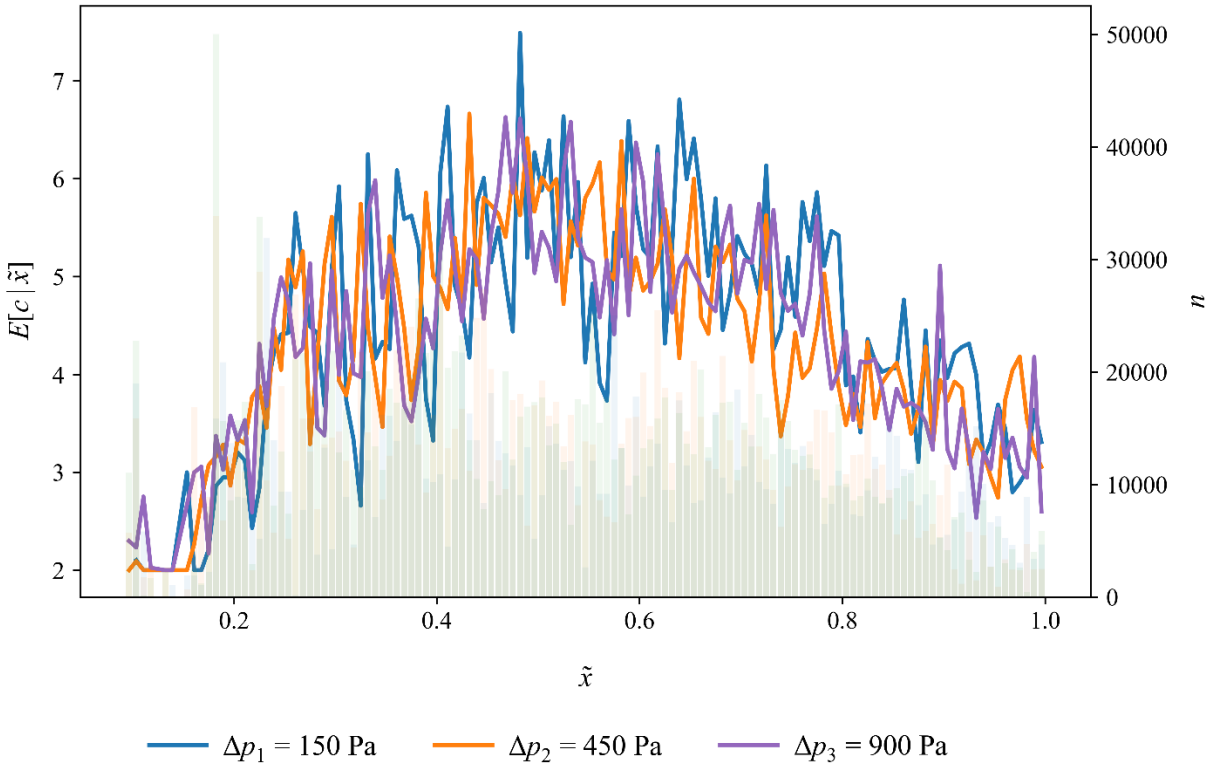

Fig. S2. Streamwise mean coordination number for the stabilised skeleton subset over the stabilised window.

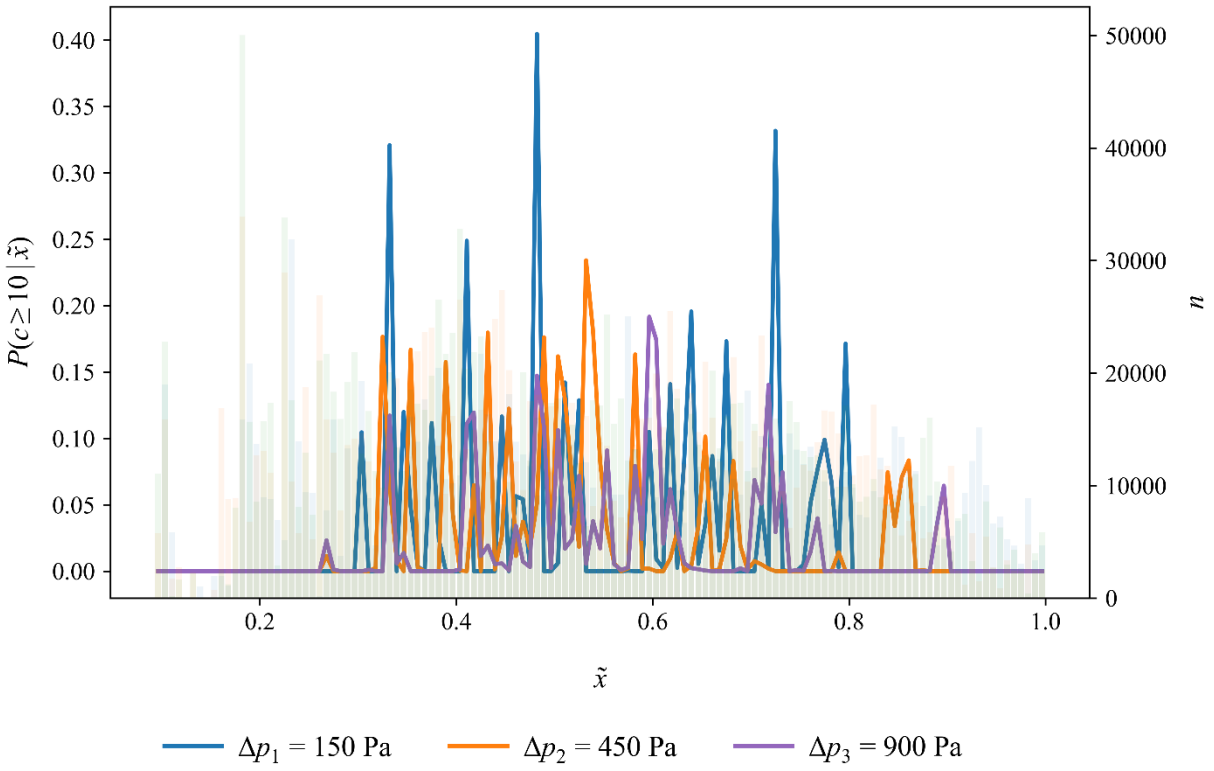

Fig. S3. Streamwise exceedance of highly coordinated contacts for the stabilised skeleton subset over the stabilised window.

Appendix B: Supplementary sensitivity analyses

This appendix provides supporting sensitivity checks for the main-paper perimeter-tail interpretation. Fig. S4 shows baseline 10% perimeter-band results for the normal component in (a) P99, (b) P99.5, and (c) $E(\sigma_n \geq 2{,}000\ \text{Pa})$ across the interior, non-corner perimeter, and corner regions. Panels (d-f) show the corresponding non-corner-perimeter-to-interior ratios across 5%, 10%, and 15% band widths. Ratios above unity indicate a stronger upper-tail response in the non-corner perimeter than in the interior. The results show that the elevated normal upper tail is not confined to corners under the baseline definition, and that the perimeter-associated contrast is retained for the 10% and 15% bands but not for the 5% band.

Table S3 reports whole-screen loaded-threshold sensitivity when the loaded-facet threshold is increased from 0 Pa to 1 Pa. Whole-screen f_L and μ_{active} are reported for the normal and shear components at both threshold definitions. The changes are negligible, which confirms that the reported decomposition is not sensitive to the zero-threshold choice.

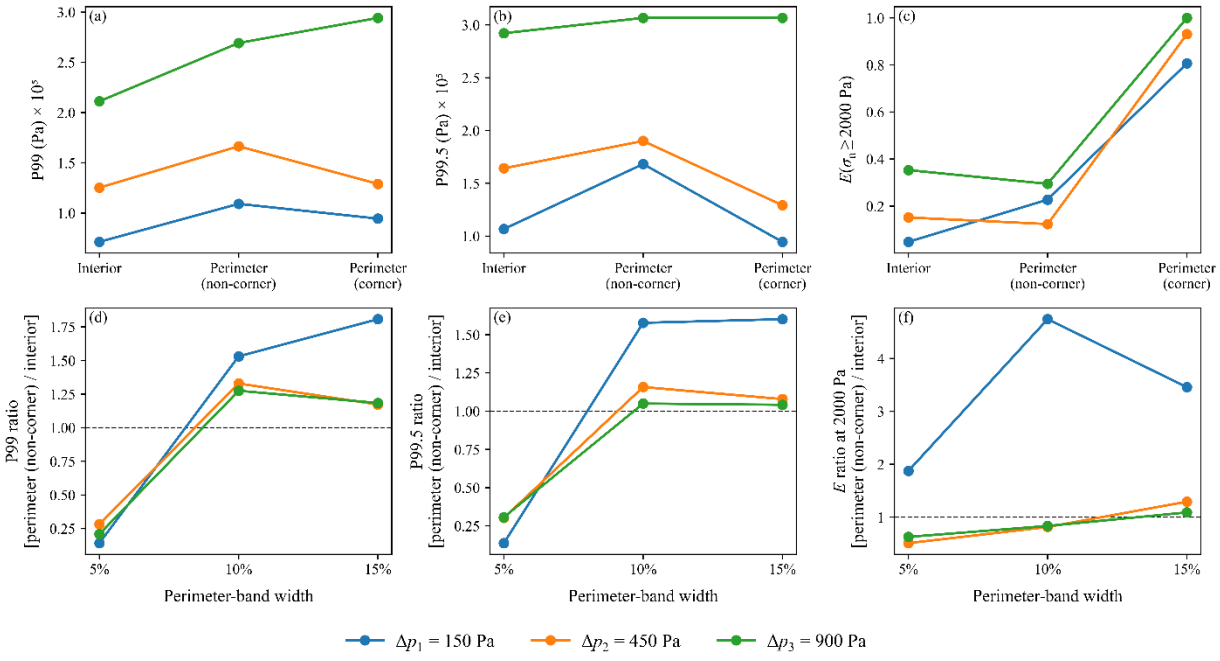

Fig. S4. Perimeter-band sensitivity for (a) P99, (b) P99.5, (c) $E(\sigma_n \geq 2{,}000\ \text{Pa})$, and (d-f) non-corner-perimeter-to-interior ratios.

Table S3. Computational-domain dimensions and mean stabilised filter-bed thickness.

Case	Stress component	σ_{min} (Pa)	f_L	μ_{active} (Pa)
Δp_1	Normal	0	0.0572	2908
		1	0.0568	2928
	Shear	0	0.0572	606
		1	0.0542	639
Δp_2	Normal	0	0.0661	4964
		1	0.0660	4969
	Shear	0	0.0661	1008
		1	0.0653	1021
Δp_3	Normal	0	0.0745	8609
		1	0.0745	8614
	Shear	0	0.0745	1741
		1	0.0738	1758